INORGANIC CHEMISTRY FRONTIERS

RESEARCH ARTICLE

View Article Online
View Journal | View Issue

Cite this: *Inorg. Chem. Front.*, 2024, **11**, 8770

Unprecedented aluminum molecular ring based-layer with tailorable optical limiting effect†

Lin Geng,‡[a] Di Wang,‡[b] Ran-Qi Chen,[a] San-Tai Wang,[a] Chan Zheng, *[b] Wei-Hui Fang *[a] and Jian Zhang [a]

Received 5th October 2024,
Accepted 28th October 2024

DOI: 10.1039/d4qi02507e

rsc.li/frontiers-inorganic

The uncontrolled assembly of Al(III) octahedra makes the synthesis of related two-dimensional (2D) compounds unpredictable, thus limiting their potential applications. In contrast to traditional synthesis methods, we propose a stepwise synthetic approach based on aluminum molecular rings. By fine-tuning the angle of the coordination unit and direction of anchoring modulation, a zero-dimensional (0D) aluminum molecular ring (**AlOC-196**) can be successfully preserved as a unique building block, allowing for the construction of a targeted 2D configuration (**AlOC-197**). Notably, the weak interlayer interactions facilitate its further exfoliation process. Moreover, compared to bulk crystals, nanosheets produced through liquid-phase exfoliation exhibit enhanced third-order nonlinear optical (NLO) properties. This coordination-driven self-assembly strategy shows promise in expanding the structural diversity and functionality of layered materials.

Introduction

Two-dimensional (2D) nanomaterials (graphene, black phosphorus, hexagonal boron nitride, *etc.*) have demonstrated considerable promise across diverse fields, including optoelectronics, photonics, and bioimaging, due to their unique physical, chemical, and electronic properties.[1–4] In recent times, the emergence of crystalline 2D materials such as metal–organic frameworks (MOFs), covalent organic frameworks, and hydrogen-bonded organic frameworks has aroused significant interest.[5–10] Notably, these materials not only maintain the advantages of traditional 2D inorganic materials but also offer a highly adaptable platform for specific functional applications. In addition, precise control over the exfoliation of these crystalline materials into nanosheets is a crucial method for effectively harnessing their functional applications.[11–16] In general, exfoliated nanosheets have unique advantages over bulk crystalline materials, such as enhanced electrical conductivity, fast electron mobility, highly exposed active sites and ultra-high specific surface areas. However, exfoliation requires the material to possess an inherent stability that allows it to endure the rigorous exfoliation process. Consequently, despite the abundance of available 2D crystalline structures, there are still certain challenges present.

Aluminum-related compounds, renowned for their excellent stability and natural abundance, have undoubtedly emerged as promising representative materials.[17–21] Notably, precise manipulation of the weak interaction between the layers within the 2D structure plays a pivotal role in effectively stripping the structure. So far, most of the aluminum-based frameworks reported in the literature have been presented as three-dimensional (3D) structures.[22–25] However, achieving precise control over the synthesis of 2D aluminum-based frameworks remains challenging, and only a few examples have been reported.[26–30]

Based on our previous work on aluminum molecular rings,[31] we have implemented a coordination-driven self-assembly strategy using discrete aluminum molecular rings as a secondary building unit (SBU) to create a novel aluminum molecular ring-based layer (Scheme 1). Typically, the utilization of linkers at the *para*-position like isonicotinic acid ligands leads to the formation of 3D aluminum-based frameworks.[32–34] Bearing this in mind, we adjusted the angle of the N coordination site and chose nicotinic acid (NA) as the linker to isolate individual aluminum molecular rings of **AlOC-196**, which were then utilized as an SBU to form the layered **AlOC-197**. This marks the first instance of an aluminum molecular ring-based layer. Furthermore, its ability to exfoliate into 2D nanosheets is attributed to the controlled weak interactions and inherent stability (Scheme 1). In com-

[a]*State Key Laboratory of Structural Chemistry, Fujian Institute of Research on the Structure of Matter, Chinese Academy of Sciences, 350002 Fuzhou, P.R. China. E-mail: fwh@fjirsm.ac.cn, czheng.fjut@gmail.com*

[b]*Institute of Biology and Chemistry, Fujian University of Technology, 350118 Fuzhou, P.R. China*

†Electronic supplementary information (ESI) available. CCDC 2324132 and 2324133. For ESI and crystallographic data in CIF or other electronic format see DOI: https://doi.org/10.1039/d4qi02507e

‡These authors contributed equally to this work.

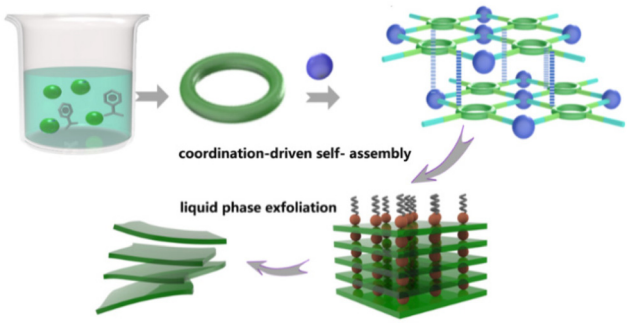

Scheme 1 Schematic diagram showing the stepwise designed synthesis of the layer compound based on the aluminum molecular ring and the liquid phase exfoliation for nanosheets.

parison to bulk crystal materials, nanosheets showed improved third-order nonlinear reverse saturation absorption (RSA) response.

Results and discussion

Reviewing past investigations on 2D aluminum-based frameworks, the inorganic SBU is typically limited to $\{AlO_6\}$ units or 1D chains (Fig. 1, Table S1†). Notably, in 2010, Riekel *et al.* employed the hydrothermal method to create the 2D Al-MOF **MIL-129**, featuring a 1D chain as the SBU.[26] This chain-type SBU was also observed in the classic **CAU-11** and **CAU-15** developed by the Stock group.[28,35] In addition, they contributed the typical $\{AlO_6\}$ SBU configuration in **CAU-20**.[27] More recently, Zhang presented the formation of layers using planar porphyrin ligands and $\{AlO_6\}$ units.[30] Nevertheless, the construction of 2D aluminum-based frameworks remains a significant challenge. On the one hand, inhibiting the 3D growth of the framework and directing it to form a 2D structure requires high adaptability tunability of the metal center and organic ligands. On the other hand, the inherent synthesis difficulties make it easy to obtain thermodynamically favorable products with simple structural types, which leads to some challenges in enriching the structural diversity of SBUs.

Building on our previous studies on aluminum molecular rings, we have demonstrated that the cluster core of aluminum rings can be retained even after functional ligand modifications. Utilizing this as the SBU could potentially allow for the manipulation of higher-dimensional MOFs by adjusting the linker while accurately retaining the SBU configuration, thereby mitigating the complexity in design to some extent. Additionally, incorporating aluminum molecular rings with multiple coordination sites into frameworks can facilitate modulation interactions to adapt to the 2D configuration. Based on the above considerations, the nicotinic acid was chosen as the ligand for constructing an additional coordination site on the aluminum ring. Most importantly, a distinct distortion angle between the –N atomic site and the carboxylic acid site within the nicotinic acid ligand is pivotal for achieving the layer assembly.

Given the significant challenge posed by the facile hydrolysis of aluminum(III) in synthesis, the organic aluminum salt (aluminum isopropoxide, $Al(O^iPr)_3$) and organic phase solvent (propanol) have been selected. Furthermore, prolonging the synthesis time has also contributed to the crystallization. Colourless crystals of $H[Al_8(NA)_{12}(\mu\text{-}OH)_4(OPr^n)_8(Cl)]\cdot 4(C_3H_7OH)(H_2O)$, namely **AlOC-196**, were isolated through the solvothermal reaction of $Al(O^iPr)_3$, and nicotinic acid ligand in propanol at 100 °C. Single crystal X-ray diffraction analysis

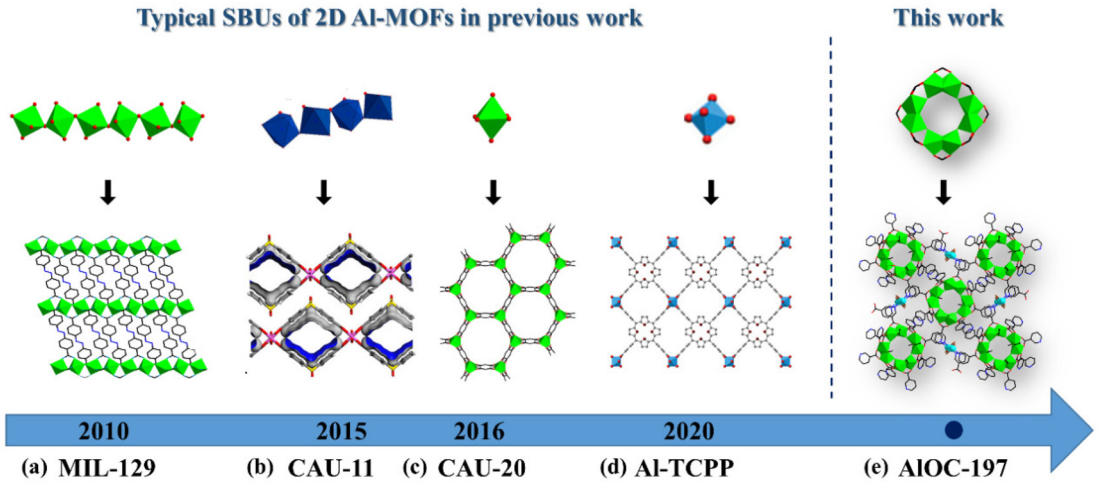

Fig. 1 Comparison diagram of typical SBU units in 2D Al-MOF in previous work and this work. (a) Crystal structure of **MIL-129** with 1D chain as SBU.[26] (b) Crystal structure of **CAU-11** with 1D chain as SBU.[28] Reproduced from ref. 28 with permission from American Chemical Society, Copyright 2014. (c) Crystal structure of **CAU-20** with $\{AlO_6\}$ as SBU.[27] (d) Crystal structure of **Al-TCPP** with $\{AlO_6\}$ as SBU.[30] (e) The crystal structure of **AlOC-197** constructed with aluminum molecular ring in this work. Color code: green/blue/sky blue is Al, light blue is Cu, red is O, blue is N, black/gray is C, and brown is Cl (the H atoms are omitted for clarity).

showed that **AlOC-196** crystallized in the $P2_1/c$ space group (Fig. S1†). As shown in Fig. 2a, the eight-membered ring **AlOC-196** was composed of eight hexa-coordinate Al^{3+} ions, 12 deprotonated nicotinic acid ligands, 8 deprotonated propanol molecules, and 4 bridged hydroxyl groups. The cluster core can be seen as 4 groups of edge shared $\{Al_2\}$ units (Fig. S2†) bridged by 4 hydroxyl groups in a common vertex manner and the inner diameter of the cluster is about 5.8 Å. Each group of the 12 deprotonated nicotinic acid ligands is located at two bipolar and equatorial positions of the molecular ring, respectively. From the side view, the outer diameter of **AlOC-196** reaches 21.3 Å and the thickness is about 11.2 Å (Fig. 2a). It is noteworthy that upon meticulous examination of the 3D stacking mode of **AlOC-196**, a conspicuous spatial separation is discerned between adjacent aluminum molecular rings (Fig. S3†). Interestingly, nicotinic acid ligands on adjacent clusters exhibit a notable tendency to align in a "head-to-head" orientation, with the distance between N–N measured about 9.6 Å (Fig. 2a). This unoccupied site suggests the potential for anchoring metal ions, which facilitates the targeted expansion of discrete aluminum molecular rings into a 2D configuration.

For the purpose of effectively anchoring the free –N site in nicotinic acid linker, the metal copper ion was chosen owing to its commendable nitrophilicity (Fig. 2b). Thus, the metal salt of cuprous chloride (CuCl) was introduced during synthesis through the one-step method.

Also, triethylamine was included as an alkaline regulator to facilitate crystallization and serve as a template for modulating the spacing between layers. Single crystal X-ray diffraction analysis revealed that the 2D configuration of blocky crystal **AlOC-197** (Fig. 2b, Table S2†) crystallized in the $P2_1/c$ space group with the molecular formula $[Al_8Cu^{II}Cu^{I}Cl_2(NA)_{12}(\mu\text{-}OH)_4(OPr^n)_8(Cl)]\cdot 10(H_2O)$. Different from the traditional SBUs in aluminum-based MOFs (discrete metal nodes or 1D chain), 2D network **AlOC-197** consists of aluminum molecular rings $\{Al_8\}$ as SBUs connected copper–halide cluster $\{Cu_2Cl_2\}$ through nicotinic acid ligands (Fig. 2b). Notably, the construction unit of $\{Al_8\}$ is consistent with the isolated rings of **AlOC-196**. And the nodes of the copper–halide clusters $\{Cu_2Cl_2\}$ generated *in situ* act as "bridges" to directional anchors the $\{Al_8\}$ rings, demonstrating the feasibility of the coordination-driven self-assembly strategy. As shown in Fig. 2b, the problem of the distribution of Cu/Cl occupancy on the crystallography is mainly attributed to the partial defects of the crystal itself. Since the 2D structure is induced by weak interlayer interactions, it may usually lead to disordered stacking between layers and trigger crystal defects, which makes it difficult to obtain single crystals of good quality (Fig. S4†).[36] In the unit of $\{Cu_2Cl_2\}$, the valence states of the Cu ions at the sides and in the middle are +1 and +2, respectively (Fig. 2b). Cu(II) was attributed to partial oxidation during synthesis. This valence configuration was also confirmed by bond valence sum analysis (Table S3†) and the X-ray photoelectron spectroscopy (XPS) results (Fig. 3b). Moreover, the Cu–Cl bond length in the range of 2.2 Å to 2.9 Å may be caused by Jahn–Teller effect, which is consistent with the oxidation results of

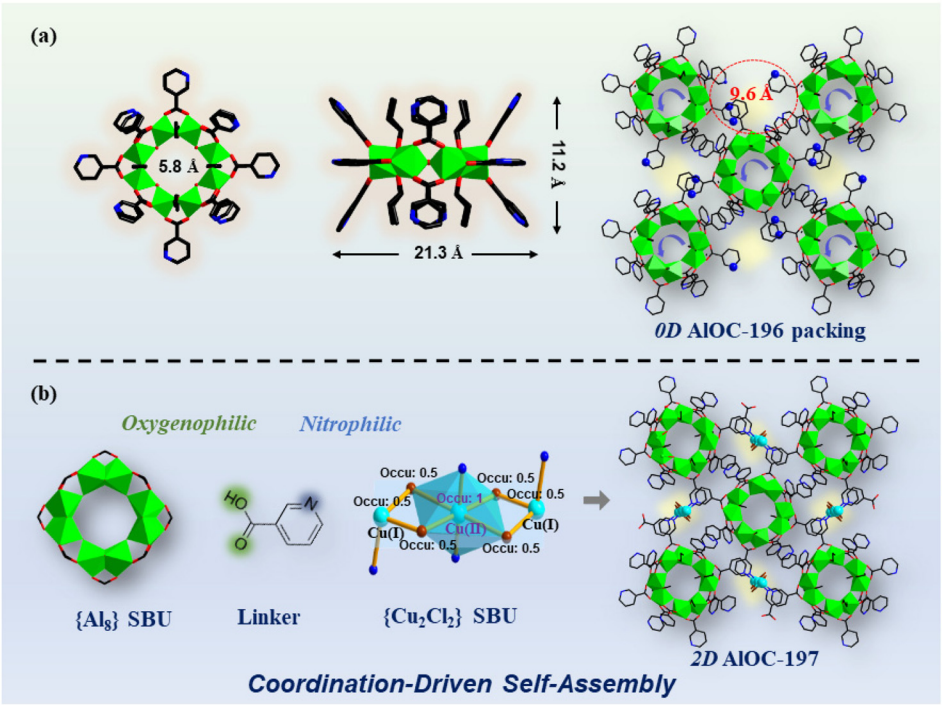

Fig. 2 Coordination-driven self-assembly from 0D aluminum molecular ring **AlOC-196** to 2D network **AlOC-197**. (a) The top view, side view, and stacking view of the **AlOC-196** cluster. (b) Assembly process and stacking view of 2D **AlOC-197** based on **AlOC-196** as SBU. Color code: green is Al, light blue is Cu, red is O, blue is N, black is C, and brown is Cl. (The H atoms are omitted for clarity.)

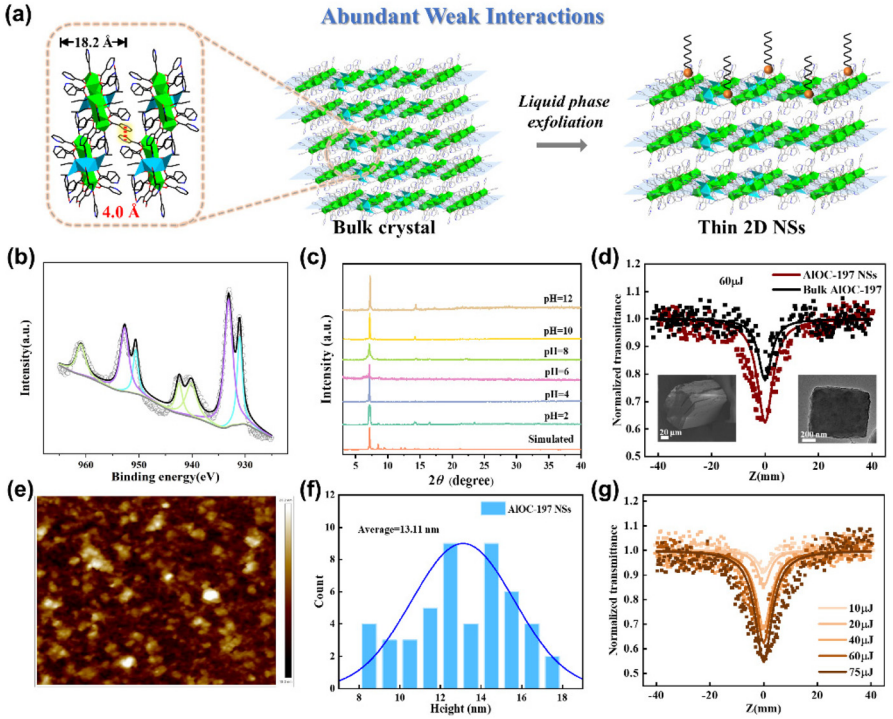

Fig. 3 (a) Schematic illustration of the liquid phase exfoliation from bulk MOF crystals to **AlOC-197** nanosheets. (b) X-ray photoelectron spectra of **AlOC-197**. (c) Chemical stability tests of **AlOC-197**, the PXRD patterns of samples treated in different pH conditions. (d) OA *Z*-scan curves of the as-synthesized **AlOC-197** bulk crystals and **AlOC-197** nanosheets under ns excitation. Inset: The SEM image of bulk crystal **AlOC-197** (left) and the TEM image of its nanosheets (right). (e) AFM image of the **AlOC-197** nanosheets. (f) The statistical analysis of the heights of **AlOC-197** nanosheets determined by AFM. (g) OA *Z*-scan curves of the **AlOC-197** nanosheets at different optical powers.

the valence state.[37] All Cl ions are bridging in **AlOC-197**. The Cu–N bond length was within the normal range of about 2.1 Å. As depicted in Fig. 2b, the $Cu^{II}Cu^{I}_{2}Cl_{4}$ clusters effectively anchor specific positions, inducing the originally discrete aluminum ring to self-adaptively twist, thereby modulating the positions of nicotinic acid ligands and further reducing the N–N distance. Accordingly, the bridging nicotinic acid ligand adopts the μ_3-η^1:η^1:η^1 coordination mode, further linking the neutral $\{Al_8\}$ ring and ultimately forming the 2D layer structure (Fig. S5†). Each $\{Al_8\}$ ring is connected to four copper halide clusters through nicotinic acid ligands at the equator. Each copper-halide cluster is connected to four $\{Al_8\}$ SBUs, thus forming a 4-connected sql topology (Fig. S6–S8†). However, considering the layered stacking growth of **AlOC-197**, there may be partial defects exist within the crystal. Hence, by combining analysis of factors such as atomic occupancy with crystallography, it is speculated that there might be partial defects in copper halide cluster nodes, possibly including $Cu^{II}Cu^{I}Cl_2$ nodes (Fig. S9 and S10†). In addition, based on the conjugation of nicotinic acid ligands, there is a π–π interaction of about 4.0 Å between adjacent 2D layers (Fig. 3a). This non-covalent interaction between molecules could expand the 2D layers into a 3D network (Fig. S8†). It is worth noting that such a weak interaction makes it possible to process low-dimensional nanosheets through external stimuli, which provides a good structural basis for subsequent processing applications.

Overall, the aluminum molecular rings that act as coordination anchors for further assembly are maintained to connect the copper–halide clusters, resulting in the architectures of **AlOC-197**. The EDS mapping of these compounds confirmed the presence of Al, C, N, O, Cu, and Cl (Fig. S9†). The presence of Cu widened the absorption band of the materials, causing them to change from colorless (**AlOC-196**, 4.03 eV) to green (**AlOC-197**, 2.78 eV) (Fig. S10 and S11†). The preservation of the $\{Al_8\}$ ring in **AlOC-197** was indicated by FT-IR spectroscopy (Fig. S12†).

SEM demonstrated the microns size of **AlOC-197** (Fig. 3d inset). The air and pH stabilities of the materials were confirmed by PXRD measurements (Fig. 3c, Fig. S13 and S14†). The thermal stability of the compounds was characterized by thermogravimetric analysis (Fig. S15†). The total solvent-accessible volumes of **AlOC-196**, and **AlOC-197**, calculated by PLATON were 21.5%, and 18.4%, respectively.

Due to the numerous π–π interactions within its 2D structure, **AlOC-197** has the potential to exhibit intriguing third-order nonlinear optical (NLO) properties.[38–44] Accordingly, open aperture (OA) *Z*-scan measurements were employed to evaluate the NLO response of **AlOC-197**. As shown in Fig. 3d, layered **AlOC-197** bulk crystals show an obvious NLO response compared to **AlOC-196**. This is predominantly due to the angle modulation of adaptive steric hindrance caused by **AlOC-197** after anchoring copper halide clusters, which results in a more

compact packing mode. Such closer packing distance (4.0 Å) and π–π interaction promote electron coupling, thereby affecting the polarizability and enhancing the third-order NLO performance (Fig. 3a). Furthermore, the incorporation of copper–halide clusters not only provides an abundance of electronic states but also effectively narrows the band gap from 4.03 eV (**AlOC-196**) to 2.78 eV (**AlOC-197**), which facilitates the electronic transitions and nonlinear effects. Given the abundant weak interactions (4 Å) between layers, there is a potential for peeling off into smaller nanosheets. Hence, the subsequent treatment of **AlOC-197** *via* liquid-phase exfoliation, aims to enhance its NLO performance (Fig. 3a). Notably, the high stability of **AlOC-197** ensured that the nanosheets maintained their integrity throughout the exfoliation process, resulting in uniform and smooth surfaces, as evidenced by the SEM and EDS image (Fig. 3d inset, Fig. S16 and S17†). The atomic force microscopy (AFM) provided further corroboration, revealing an average height of 13.11 nm and showcasing the consistent nanosheet thickness at the nanoscale (Fig. 3e and f). These findings underscore the critical importance of inherent stability and weak interactions of **AlOC-197** in producing high-quality nanosheets.

To elucidate the effect of size on the NLO performance, the NLO response of **AlOC-197** nanosheets was tested in detail. Compared to the corresponding bulk **AlOC-197** suspension, the exfoliated nanosheets exhibited significantly enhanced NLO performance (Fig. 3d). This enhancement could be attributed to the material's increased surface area and uniform structure, leading to more efficient NLO properties. Furthermore, detailed experimentation with incident pulse energy under nanosecond excitation was conducted for the **AlOC-197** nanosheets (Fig. 3g). Under ns laser pulses, a symmetric valley around $Z = 0$ appears, indicating a typical RSA effect, with the normalized transmittance rapidly decreasing as the sample passed through the focal point, intensifying as the laser input energy increased. Furthermore, a thorough analysis was conducted to elucidate the mechanisms underlying this phenomenon. The band gap of the **AlOC-197** nanosheets is approximately 3.18 eV, which is higher than the excitation energy ($h\nu < E_g < 2h\nu$ for one photon at 532 nm) (Fig. S18†). This indicates that the observed RSA response can be attributed to the two-photon absorption (TPA) mechanism. TPA is an NLO effect where ground-state electrons simultaneously absorb two photons, transitioning to the excited state *via* a virtual state.[45–48] Similar behavior has been observed in many typical sheet materials, such as graphene, $MoSe_2$, GeSe, SnSe, *etc*. Additionally, to evaluate the NLO performance of **AlOC-197** nanosheets, their NLO parameters were compared with those of other low-dimensional materials as outlined in Tables S4 and S5.† The findings indicate that the NLO characteristics of the **AlOC-197** nanosheets are comparable to or exceed the reported values for $MoSe_2$ nanosheets, Sb nanosheets, GeSe nanosheets, SnSe nanosheets, C_{60}, BN nanosheets, and CuS nanosheets.[49–55] Hence, the NLO performance of eco-friendly **AlOC-197** nanosheets has significantly improved, rendering a promising for utilization in photonic devices.

Conclusions

In conclusion, we present a straightforward coordination-driven anchoring site design strategy to expand the 0D aluminum molecular ring (**AlOC-196**) as a structural building unit to form a 2D aluminum-based framework (**AlOC-197**). Furthermore, the stable **AlOC-197** allows for efficient exfoliation from bulk crystals into high-quality nanosheets, thereby enhancing nonlinear optical absorption and demonstrating potential in optoelectronic applications such as optical switching, modulation, and laser protection. With the feasibility of the coordination-driven self-assembly strategy, the structural diversity of 2D aluminum metal–organic frameworks can be expanded through controlled anchoring of metal sites.

Data availability

X-ray crystallographic data for the structures reported in the article have been deposited at the Cambridge Crystallographic Data Centre, under deposition numbers CCDC 2324132 (**AlOC-196**), and 2324133 (**AlOC-197**). Copies of the data can be obtained free of charge *via* **https://www.ccdc.cam.ac.uk/structures/**. All data supporting this study are available within the paper and its ESI,† and from the corresponding author.

Author contributions

All authors contributed extensively to the work presented in this paper. W.-H. Fang, J. Zhang and C. Zheng conceived the research project. L. Geng, R.-Q. Chen and S. T. Wang performed the synthesis and characterization experiments. D. Wang performed NLO experiments. W.-H. Fang and L. Geng wrote the manuscript and the ESI† with input from the other authors.

Conflicts of interest

The authors declare no competing interests.

Acknowledgements

This work is supported by the National Natural Science Foundation of China (22371278, U23A2095), the Natural Science Foundation of Fujian Province (2021J06035) and Youth Innovation Promotion Association CAS (Y2021081).

References

1 H. Jin, C. Guo, X. Liu, J. Liu, A. Vasileff, Y. Jiao, Y. Zheng and S. Z. Qiao, Emerging two-dimensional nanomaterials for electrocatalysis, *Chem. Rev.*, 2018, **118**, 6337–6408.

2 T. Li, T. Jing, D. Rao, S. Mourdikoudis, Y. Zuo and M. Wang, Two-dimensional materials for electrocatalysis and energy storage applications, *Inorg. Chem. Front.*, 2022, **9**, 6008–6046.
3 Y. Chen, Z. Fan, Z. Zhang, W. Niu, C. Li, N. Yang, B. Chen and H. Zhang, Two-dimensional metal nanomaterials: synthesis, properties, and applications, *Chem. Rev.*, 2018, **118**, 6409–6455.
4 Y. L. Liu, S. Z. Zhan, G. H. Zhang, X. Y. Tao, K. Hu, D. F. Luo, L. Dang, S. K. Ng and D. Li, 2D coordination sheets based on tetranuclear cuprofullerene pentafluorobenzoate and their electronic properties, *Inorg. Chem. Front.*, 2023, **10**, 1731–1738.
5 R. Dong and X. Feng, Making large single crystals of 2D MOFs, *Nat. Mater.*, 2021, **20**, 122–123.
6 A. Schoedel, M. Li, D. Li, M. O'Keeffe and O. M. Yaghi, Structures of metal–organic frameworks with rod secondary building units, *Chem. Rev.*, 2016, **116**, 12466–12535.
7 C. Yang, X. Xu and B. Yan, A two-dimensional luminescent HOF containing an interpenetrating network structure with dual function: highly sensitive detection of methotrexate and multi-level information encryption, *Inorg. Chem. Front.*, 2023, **10**, 2951–2960.
8 Z. Q. Yao, K. Wang, R. Liu, Y. J. Yuan, J. J. Pang, Q. W. Li, T. Y. Shao, Z. G. Li, R. Feng, B. Zou, W. Li, J. Xu and X. H. Bu, Dynamic full-color tuning of organic chromophore in a multi-stimuli-responsive 2D flexible MOF, *Angew. Chem., Int. Ed.*, 2022, **61**, e202202073.
9 J. Liu, X. Y. Ren, Y. Yan, N. Wang, S. Wang, H. Zhang, J. Li and J. Yu, A new two-dimensional layered germanate with *in situ*, embedded carbon dots for optical temperature sensing, *Inorg. Chem. Front.*, 2018, **5**, 139–144.
10 C. Gao, J. Zhou, M. Cui, D. Chen, L. Zhou, F. Li and X. L. Li, Distinct nonlinear optical responses in three pairs of 2D homochiral Ag(i) enantiomers modulated by dicarboxylic acid ligands, *Inorg. Chem. Front.*, 2022, **9**, 284–293.
11 W. Xia, J. Tang, J. Li, S. Zhang, K. C. W. Wu, J. He and Y. Yamauchi, Defect-rich graphene nanomesh produced by thermal exfoliation of metal–organic frameworks for the oxygen reduction reaction, *Angew. Chem., Int. Ed.*, 2019, **58**, 13354–13359.
12 J. Kang, V. K. Sangwan, J. D. Wood and M. C. Hersam, Solution-based processing of monodisperse two-dimensional nanomaterials, *Acc. Chem. Res.*, 2017, **50**, 943–951.
13 M. Li, C. Ma, X. Liu, J. Su, X. Cui and Y. He, Synthesis of a 2D phosphorus material in a MOF-based 2D nano-reactor, *Chem. Sci.*, 2018, **9**, 5912–5918.
14 Y. Ding, Y. P. Chen, X. Zhang, L. Chen, Z. Dong, H. L. Jiang, H. Xu and H. C. Zhou, Controlled intercalation and chemical exfoliation of layered metal–organic frameworks using a chemically labile intercalating agent, *J. Am. Chem. Soc.*, 2017, **139**, 9136–9139.
15 R. J. Wei, P. Y. You, H. Duan, M. Xie, R. Q. Xia, X. Chen, X. Zhao, G. H. Ning, A. I. Cooper and D. Li, Ultrathin metal–organic framework nanosheets exhibiting exceptional catalytic activity, *J. Am. Chem. Soc.*, 2022, **144**, 17487–17495.
16 Y. Huang, Y. H. Pan, R. Yang, L. H. Bao, L. Meng, H. L. Luo, Y. Q. Cai, G. D. Liu, W. J. Zhao, Z. Zhou, L. M. Wu, Z. L. Zhu, M. Huang, L. W. Liu, L. Liu, P. Cheng, K. H. Wu, S. B. Tian, C. Z. Gu, Y. G. Shi, Y. F. Guo, Z. G. Cheng, J. P. Hu, L. Zhao, G. H. Yang, E. Sutter, P. Sutter, Y. L. Wang, W. Ji, X. J. Zhou and H. J. Gao, Universal mechanical exfoliation of large-area 2D crystals, *Nat. Commun.*, 2020, **11**, 2453.
17 W. H. Fang, Y. L. Xie, S. T. Wang, Y. J. Liu and J. Zhang, Induced aggregation, solvent regulation, and supracluster assembly of aluminum oxo clusters, *Acc. Chem. Res.*, 2024, **57**, 1458–1466.
18 D. Luo, F. Wang, C. H. Liu, S. T. Wang, Y. Y. Sun, W.-H. Fang and J. Zhang, Combination of aluminum molecular rings with chemical reduction centers for iodine capture and aggregation, *Inorg. Chem. Front.*, 2022, **9**, 4506–4516.
19 S. Bureekaew, S. Horike, M. Higuchi, M. Mizuno, T. Kawamura, D. Tanaka, N. Yanai and S. Kitagawa, One-dimensional imidazole aggregate in aluminium porous coordination polymers with high proton conductivity, *Nat. Mater.*, 2009, **8**, 831–836.
20 Y. Zhang, Q.-H. Li, W.-H. Fang and J. Zhang, Aluminum molecular rings bearing amino-polyalcohol for iodine capture, *Inorg. Chem. Front.*, 2022, **9**, 592–598.
21 Y. J. Liu, H. F. Su, Y. F. Sun, S. T. Wang, C. Y. Zhang, W. H. Fang and J. Zhang, Supracluster assembly of archimedean cages with 72 hydrogen bonds for the aldol addition reaction, *Angew. Chem., Int. Ed.*, 2023, **62**, e202309971.
22 W. Fan, K. Y. Wang, C. Welton, L. Feng, X. Wang, X. Liu, Y. Li, Z. Kang, H. C. Zhou, R. Wang and D. Sun, Aluminum metal–organic frameworks: From structures to applications, *Coord. Chem. Rev.*, 2023, **489**, 215715.
23 N. Stock, Metal-organic frameworks: aluminium-based frameworks, in *Encyclopedia of Inorganic and Bioinorganic Chemistry*, 2014, pp. 1–16. DOI: **10.1002/9781119951438.eibc2197**.
24 D. Alezi, Y. Belmabkhout, M. Suyetin, P. M. Bhatt, L. J. Weselinski, V. Solovyeva, K. Adil, I. Spanopoulos, P. N. Trikalitis, A. H. Emwas and M. Eddaoudi, MOF crystal chemistry paving the way to gas storage needs: aluminum-based soc-MOF for CH_4, O_2, and CO_2 Storage, *J. Am. Chem. Soc.*, 2015, **137**, 13308–13318.
25 L. Li, S. L. Xiang, S. Q. Cao, J. Y. Zhang, G. F. Ouyang, L. P. Chen and C. Y. Su, A synthetic route to ultralight hierarchically micro/mesoporous Al(III)-carboxylate metal-organic aerogels, *Nat. Commun.*, 2013, **4**, 1774.
26 C. Volkringer, T. Loiseau, T. Devic, G. Férey, D. Popov, M. Burghammer and C. Riekel, A layered coordination polymer based on an azodibenzoate linker connected to aluminium (MIL-129), *CrystEngComm*, 2010, **12**, 3225–3228.
27 S. Halis, A. K. Inge, N. Dehning, T. Weyrich, H. Reinsch and N. Stock, Dihydroxybenzoquinone as linker for the syn-

thesis of permanently porous aluminum metal–organic frameworks, *Inorg. Chem.*, 2016, **55**, 7425–7431.
28 N. Reimer, H. Reinsch, A. K. Inge and N. Stock, New Al-MOFs based on sulfonyldibenzoate ions: a rare example of intralayer porosity, *Inorg. Chem.*, 2014, **54**, 492–501.
29 J. M. Moreno, A. Velty, U. Díaz and A. Corma, Synthesis of 2D and 3D MOFs with tuneable Lewis acidity from preformed 1D hybrid sub-domains, *Chem. Sci.*, 2019, **10**, 2053–2066.
30 M. Jian, R. Qiu, Y. Xia, J. Lu, Yu Chen, Q. Gu, R. Liu, C. Hu, J. Qu, H. Wang and X. Zhang, Ultrathin water-stable metal-organic framework membranes for ion separation, *Sci. Adv.*, 2020, **6**, eaay3998.
31 L. Geng, C. H. Liu, S. T. Wang, W. H. Fang and J. Zhang, Designable aluminum molecular rings: ring expansion and ligand functionalization, *Angew. Chem., Int. Ed.*, 2020, **59**, 16735–16740.
32 C. H. Liu, W. H. Fang, Y. Sun, S. Yao, S. T. Wang, D. Lu and J. Zhang, Designable assembly of aluminum molecular rings for sequential confinement of iodine molecules, *Angew. Chem., Int. Ed.*, 2021, **60**, 21426–21433.
33 W. Lv, Y. J. Ma, A. N. Wang, Y. Mu, S. W. Niu, L. Wei, W. L. Dong, X. Y. Ding, Y. B. Qiang, X. Y. Li and G. M. Wang, Al_8 custer-based metal halide frameworks: balancing singlet–triplet excited states to ahieve white light and multicolor luminescence, *Small*, 2023, **20**, 2306713.
34 H. Xu, Y. Wu, L. Yang, Y. Rao, J. Wang, S. Peng and Q. Li, Water-harvesting metal–organic frameworks with gigantic Al_{24} units and their deconstruction into molecular clusters, *Angew. Chem., Int. Ed.*, 2022, **62**, e202217864.
35 H. Reinsch, D. D. Vos and N. Stock, Structure and properties of $[Al_4(OH)_8(o\text{-}C_6H_4(CO_2)_2)_2]\cdot H_2O$, a layered aluminum phthalate, *Z. Anorg. Allg. Chem.*, 2013, **639**, 2785–2789.
36 J. H. Dou, M. Q. Arguilla, Y. Luo, J. Li, W. Zhang, L. Sun, J. L. Mancuso, L. Yang, T. Chen, L. R. Parent, G. Skorupskii, N. G. Libretto, C. Sun, M. C. Yang, P. V. Dip, E. J. Brignole, J. T. Miller, J. Kong, C. H. Hendon, J. Sun and M. Dincă, Atomically precise single-crystal structures of electrically conducting 2D metal–organic frameworks, *Nat. Mater.*, 2021, **20**, 222–228.
37 W. M. Leovac, M. D. Joksović, V. Divjaković, Ž. Šaranović and A. Pevec, Synthesis, spectroscopic and X-ray characterization of a copper(II) complex with the Schiff base derived from pyridoxal and aminoguanidine: NMR spectral studies of the ligand, *J. Inorg. Biochem.*, 2007, **101**, 1094–1097.
38 Y. Li, C. Zheng, S. T. Wang, Y. J. Liu, W. H. Fang and J. Zhang, Record aluminum molecular rngs for optical limiting and nonlinear optics, *Angew. Chem., Int. Ed.*, 2022, **61**, e202116563.
39 S. T. Wang, W. H. Fang and J. Zhang, Meltable aluminum molecular rings with fluorescence and nonlinear optical properties, *Angew. Chem., Int. Ed.*, 2024, **63**, E202400161.
40 S. J. Bao, Z. M. Xu, Z. W. Huang, T. C. Yu, M. Y. Wang, Y. L. Song, Z. Niu, B. F. Abrahams and J. P. Lang, A hierarchical supramolecular assembly strategy for remarkably amplifying third-order nonlinear optical responses of clusters, *Sci. China Mater.*, 2023, **66**, 3278–3284.
41 R. Medishetty, J. K. Zaręba, D. Mayer, M. Samoć and R. A. Fischer, Nonlinear optical properties, upconversion and lasing in metal–organic frameworks, *Chem. Soc. Rev.*, 2017, **46**, 4976–5004.
42 B. Li, H. Li, C. Wu, L. L. Fu, D. W. Boukhvalov, M. G. Humphrey, C. Zhang and Z. Huang, Unlocking giant third-order optical nonlinearity in $(MA)_2CuX_4$ through Introducing Jahn-Teller distortion, *Angew. Chem., Int. Ed.*, 2024, e202406941.
43 S. T. Wang, X. Qi, R. Q. Chen, W. H. Fang and J. Zhang, Two solvent-dependent Al_{16} nanorings: design, synthesis and nonlinear optical limiting behavior, *Inorg. Chem. Front.*, 2024, **11**, 462–469.
44 Z. H. Liu, S. H. Shen, C. Y. Zhang, J. Niu, Q. H. Li, J. Zhang and W. H. Fang, Design and synthesis of a deep-cavity aluminium-organic macrocycle to trap dyes and generate enhanced non-linear optical performance, *Inorg. Chem. Front.*, 2024, **11**, 3777–3785.
45 S. C. Wang, Q. S. Zhang, Z. Wang, L. Zheng, X. D. Zhang, Y. N. Fan, H. Y. Fu, X. H. Xiong and M. Pan, One and two-photon excited fluorescence optimization of metal-organic frameworks with symmetry-Reduced AIEgen-ligand, *Angew. Chem., Int. Ed.*, 2022, **61**, e202211356.
46 J. Chen, W. Zhang and T. Pullerits, Two-photon absorption in halide perovskites and their applications, *Mater. Horiz.*, 2022, **9**, 2255–2287.
47 Z. Wang, C.-Y. Zhu, J.-T. Mo, P.-Y. Fu, Y.-W. Zhao, S.-Y. Yin, J.-J. Jiang, M. Pan and C.-Y. Su, White-light emission from dual-way photon energy conversion in a dye-encapsulated metal-organic framework, *Angew. Chem., Int. Ed.*, 2019, **58**, 9752.
48 P.-Y. Fu, S.-Z. Yi, Z.-H. Wang, J.-Y. Zhuang, Q.-S. Zhang, J.-T. Mo, S.-C. Wang, H. Zheng, M. Pan and C.-Y. Su, One/two-photon-excited eSIPT-attributed coordination polymers with wide temperature range and color-tunable long persistent luminescence, *Angew. Chem., Int. Ed.*, 2023, **62**, e202309172.
49 H. Pan, H. Chu, Y. Li, S. Zhao and D. Li, Comprehensive study on the nonlinear optical properties of few-layered MoSe2 nanosheets at 1 μm, *J. Alloys Compd.*, 2019, **806**, 52–57.
50 L. Zhang, S. Fahad, H. R. Wu, T. T. Dong, Z. Z. Chen, Z. Q. Zhang, R. T. Liu, X. P. Zhai, X. Y. Li, X. Fei, Q. W. Song, Z. J. Wang, L. C. Chen, C. L. Sun, Y. Peng, Q. Wang and H. L. Zhang, Tunable nonlinear optical responses and carrier dynamics of two-dimensional antimonene nanosheets, *Nanoscale Horiz.*, 2020, **5**, 1420–1429.
51 J. Mu, Z. Yang, Q. Zhang, X. Yuan, G. Wang, H. Qi, F. Wang and W. Sun, Thickness-dependent ultrafast nonlinear optical response of germanium selenide nanosheets, *J. Mater. Sci.*, 2023, **58**, 11527–11538.
52 Y. Ye, Y. Xian, J. Cai, K. Lu, Z. Liu, T. Shi, J. Du, Y. Leng, R. Wei, W. Wang, X. Liu, G. Bi and J. Qiu, Linear and non-

linear optical properties of few-layer exfoliated SnSe nanosheets, *Adv. Opt. Mater.*, 2019, **7**, 1800579.
53 Y. Chen, T. Bai, N. Dong, F. Fan, S. Zhang, X. Zhuang, J. Sun, B. Zhang, X. Zhang, J. Wang and W. J. Blau, Graphene and its derivatives for laser protection, *Prog. Mater. Sci.*, 2016, **84**, 118–157.
54 F. Ma, M. Wang, Y. Shao, L. Wang, Y. Wu, Z. Wang and X. Hao, Thermal substitution' for preparing ternary BCN nanosheets with enhanced and controllable nonlinear optical performance, *J. Mater. Chem. C*, 2017, **5**, 2559–2565.
55 N. Ahmad, A. M. Alshehri, Z. R. Khan, S. A. M. Almahdawi, M. Shkir, P. M. Z. Hasan, A. Alshahrie, F. Khan and A. AlAhmed, An investigation on structural, optical and enhanced third order nonlinear optical properties of facilely synthesized Ce:CuS nanosheets, *Inorg. Chem. Commun.*, 2022, **139**, 109363.